Supporting information

C_3N_2: The Missing Part of Highly Stable Porous Graphitic Carbon Nitride Semiconductors

Xinyong Cai,[a] Jiao Chen,[a] Hongyan Wang [a,*], Yuxiang Ni,[a] Yuanzheng Chen[a,b,*], R. Bruce King[c,*]

[a] *School of Physical Science and Technology, Key Laboratory of Advanced Technology of Materials, Ministry of Education of China, Southwest Jiaotong University, Chengdu 610031*

[b] *Beijing Computational Science Research Center, Haidian District, Beijing 100193, China*

[c] *Department of Chemistry and Center for Computational Chemistry, University of Georgia, Athens, Georgia 30602, USA*

E-mail: (H.W) hongyanw@swjtu.edu.cn; (Y. C.) cyz@swjtu.edu.cn; (R. B. K) rbking@uga.edu

Index Page

1. Design scheme s3

2. Computational details s7

3. Atomic configurations for C_3N, C_2N-h2D, and T-C_3N_2 ..... s8

4. The graphitic N concentration in CNs s9

5. ELF, Phonon spectrum and MD simulations of T-C_3N_2 monolayer s9

6. Electronic structures and the DOS of C_2N-h2D and H-C_3N_2 monolayers s10

7. The band structure of H-C_3N_2 relative to the vacuum level s11

8. The different stacking bilayers of H-C_3N_2 and T-C_3N_2 ..... s11

9. The differential charge density of AA and AA' stacking bilayers T-C_3N s13

10. Carrier effective masses, in-plane stiffness, and the deformation potential

constant..s13

11. References s14

Design scheme

Porous graphitic carbon nitride (PGCN) monolayers are typically synthesized by pyrolytic elimination of ammonia from molecular building blocks of planar hexagonal rings with pendant amino substituents. The nitrogen atoms remaining from some of the original amino substituents after the ammonia elimination become the linkers between the building blocks in the 2D PGCN monolayer. Three-fold symmetry of the building blocks is necessary for an infinite graphite-like structure. The synthesized CNs are C_3N_5, C_3N_4, C_3N_3, and C_3N. Interestingly, we found the ratio of C_3N_2 can forms the C_3N_m family (m=5, 4, 3, 2, 1) with the above mentioned CNs. In order to obtain a PGCN monolayer of a carbon-richer carbon nitride, such as C_3N_2 of interest in this paper, suitable building blocks with graphitic and pyridinic nitrogen atoms need to have carbon-richer hexagonal rings while retaining three-fold overall symmetry.

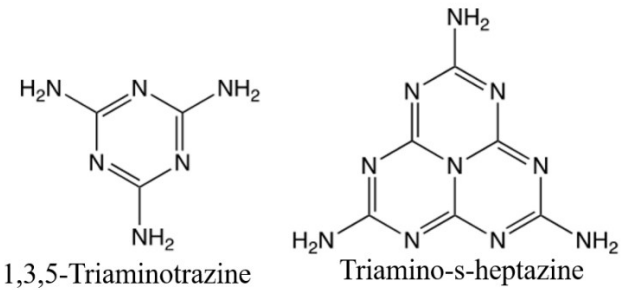

Figure S1. Symmetrical building blocks with C_3N_3 triazine rings for synthesizing C_3N_4 allotropes.

The most common building blocks for PGCN monolayers are constructed from hexagonal triazine rings consisting of alternating carbon and nitrogen atoms as exemplified by the triazine and heptazine systems in Figure S1. The C: N ratio in these building blocks leads to the stoichiometry C_3N_4 for the final polymeric carbon nitride monolayer after the elimination of all of the hydrogen atoms on the pendant amino groups as part of ammonia. This approach to the synthesis of carbon nitride monolayers leads to porous systems with porosity dependent on the choice of the building block. The carbon-nitrogen balance in building blocks for the synthesis of carbon nitride monolayers consisting exclusively of triazine rings symmetrically substituted with amino groups necessarily leads to the stoichiometry C_3N_4 for the resulting carbon nitride after pyrolytic elimination of ammonia.

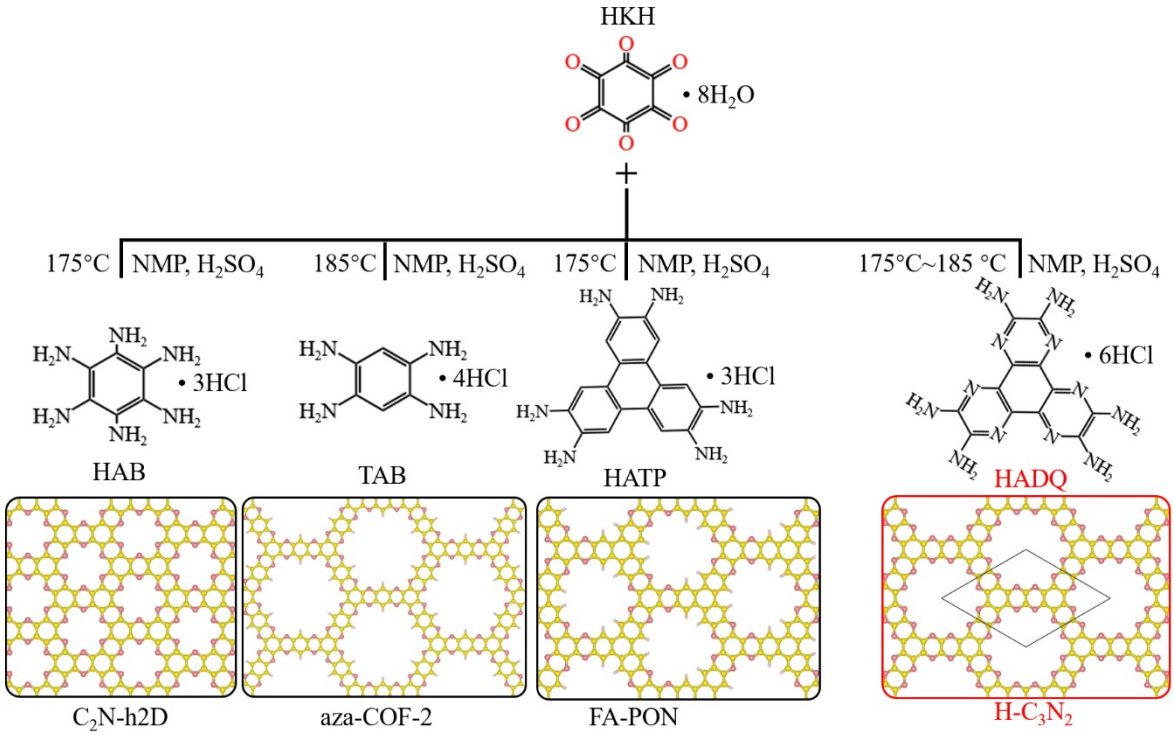

Figure S2. Schematic representation of the synthesis of C_2N-h2D, aza-COF-2, FA-PON, and a possible synthesis path of H-C_3N_2.

For g-C_3N_4, we learn that it can be synthesized by the thermal condensation of several low-cost nitrogen-rich precursors with about 550 °C such as cyanamide[1], dicyandiamide[2], melamine[3], thiourea[4], urea[5], or mixtures thereof[6]. Similar to g-C_3N_4, so far, there are two reported routes with different nitrogen-rich precursors to prepare C_2N-h2D in the experiment. One is the reaction between hexaaminobenzene (HAB) trihydrochloride (Figure 2a) and hexaketocyclohexane (HKH) octahydrate, the other is direct carbonization of the hexaazatriphenylene (HAT) precursor.[7] Besides, we know that the reaction between organic molecules with the same terminal functional groups could occur *via* a similar reaction path, which can be seen in the preparation of 2D porous structures.[8] For example, the combination between amino (e.g. HAB) and carbonyl (e.g. HKH) usually results in the dehydration reaction in the synthesis of PGCNs and covalent organic frameworks(COFs), such as C_2N-h2D[9-12], aza-COF-2[13-16], FA-PON[13, 17, 18], TQBQ-COF[19], and F-COF[20]. Though solvents and catalysts are sometimes different, primary monomers are unchanged.

Therefore, analogous to HAB and 2,3,6,7,10,11-Hexaaminotriphenylene (HATP) with the same

edge functional group(i.e. amino) in the synthesis of the 2D metal-organic frameworks (MOFs) $Co_3(HAB)_2$[21-23] and Co3(HATP)[24, 25], 2,3,6,7,10,11-hexamine dipyrazino quinoxaline (HADQ), which was first synthesized in 2021 and used to prepare the 2D MOF $Co_3(HADQ)_2$[26], is used to design and propose a possible synthesis scheme for α-C_3N_2[27] (designated as H-C_3N_2). According to the synthesis of C_2N-h2D,[10, 28] aza-COF-2[13, 14], and FA-PON[17, 18, 29](Figure S2) and their similar structural characteristics, we propose that using the main organic reactants (i.e. HADQ and HKH) and N-methyl-2-pyrrolidone (NMP) in the presence of a few drops of sulfuric acid (H_2SO_4) as catalysts could produce preliminary materials via a bottom-up wet-chemical reaction. The reaction mixture needs to be heated 175°C ~185 °C under argon or N_2 atmosphere for a period of time, which will be possibly hours or days. Then, the resultant solid can be filtered and Soxhlet extracted with water and methanol after being dried,[10, 13, 17] when it also needs likely to be freeze-dried at -120 °C under reduced pressure (0.05 mmHg) for some time.[10, 17]

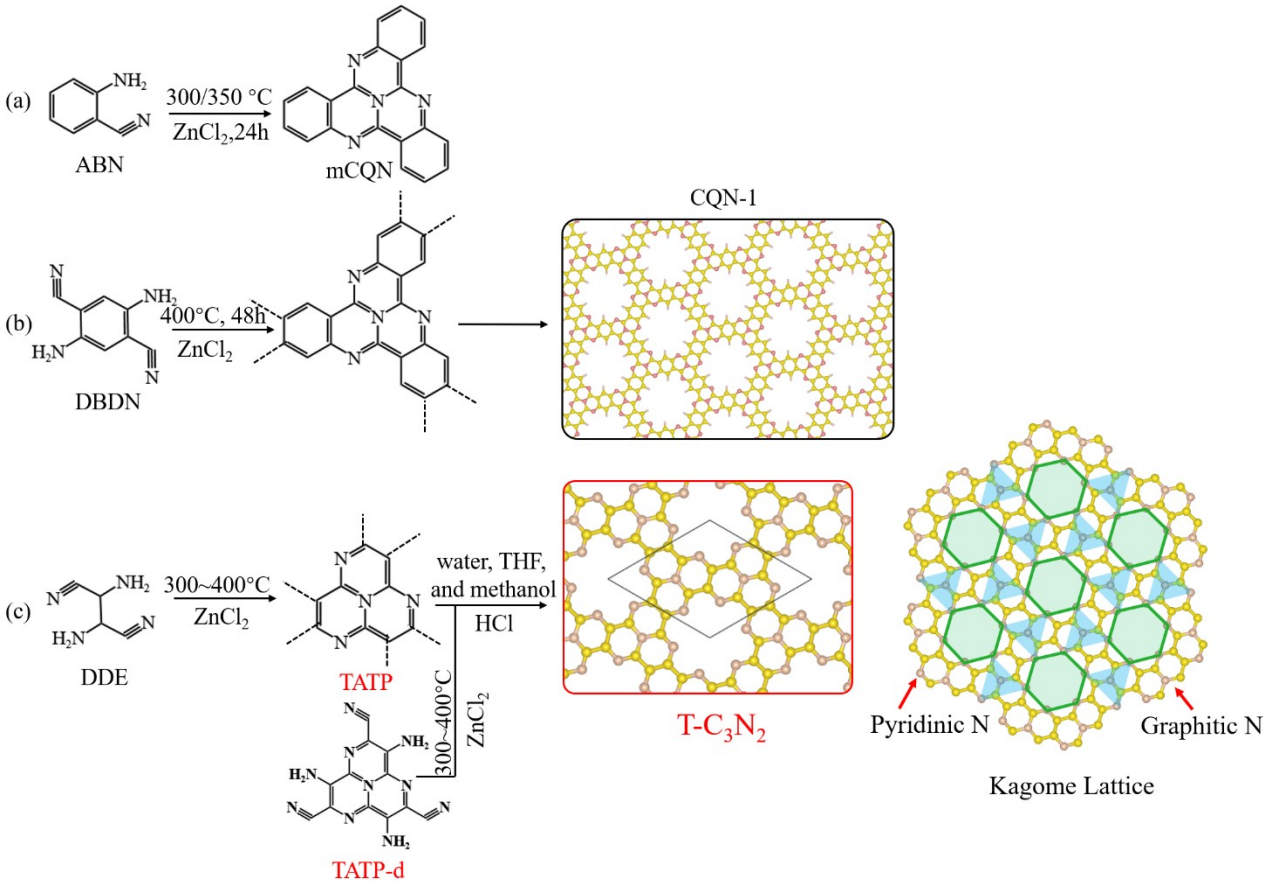

Figure S3. (a-b) The synthetic process of mCQN and CQN-1. (c) A possible scheme for the synthesis

of the T-C_3N_2 lattice by the self-assembly of DDE.

For T-C_3N_2(Figure 3S), after comparing the cohesive energy difference between it and H-C_3N_2, we find it has lower cohesive energy, which is beneficial to its realization due to the above-mentioned possibility of the preparation for H-C_3N_2. Thus we also propose a possible synthesis scheme for T-C_3N_2 based on the synthetic route of CQNs[30]. In the synthesis of mCQN and CQN-1, Zinc chloride ($ZnCl_2$) was always used as the solvent and catalyst and reacted with 2-aminobenzonitrile(ABN) and 2,5-Diamino-1,4-benzenedicarbonitrile (DBDN) for the condensation of aromatic ortho-aminonitriles to produce tricycloquinazoline linkages (Figure 3Sa-b). Similarly, our scheme is to mix 1,2-Diamino-1,2-dicyanoethylene (DDE) and anhydrous $ZnCl_2$ under 300~400 °C for a period of time. According to the reaction time of mCQN and CQN-1, the reaction time could not be for a long time. Besides, we also propose to use the derivative of TATP (TATP-d, Figure S3c) as an alternative through the same route. The reaction mixture is initially ground into fine powder and washed with water, stirred in dilute HCl solution. Again, it needs to be washed thoroughly with water, THF, and methanol, in sequence. The final product is attained after being dried under vacuum. Apart from H-C_3N_2 and T-C_3N_2, unexpectedly, the assembly of HAB and TATP could form another new C_3N_2 allotrope (designated as TH-C_3N_2, Figure 4Sa-b), and it also has a lower cohesive energy than H-C_3N_2. Through the calculation of the phonon dispersion, TH-C_3N_2 is found to be stable (Figure 4Sc), which indicates it could be synthesized in suitable experimental conditions.

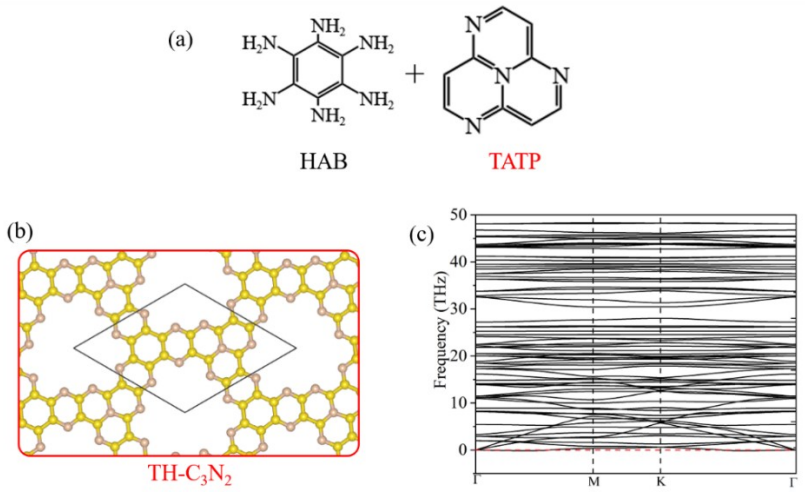

Figure S4. (a) Two possible basic organic units to produce the TH-C_3N_2 allotrope. (b-c) Structure and

Phonon spectra of the TH-C3N2.

Computational Details

CALYPSO

The particle swarm optimization (PSO) method within the evolutionary algorithm as implemented in the Crystal structure AnaLYsis by Particle Swarm Optimization (PSO) code was employed to find the lowest energy structures of $(C_3N_2)n$ (n = 1, 2, 3, 4, 5, and 6) monolayers.[31, 32] Unit cells containing 1, 2, 3, 4, 5, and 6 formula units (f.u.) were considered. In the first step, random structures with certain symmetry are constructed in which atomic coordinates are generated by the crystallographic symmetry operations. Local optimizations using the VASP code [33] were done with the conjugate gradients method and stopped when Gibbs free energy changes became smaller than 1×10^{-5} eV per cell. After processing the first-generation structures, 60% of structures with lower Gibbs free energies are selected to construct the next-generation structures by PSO. 40% of the structures in the new generation are randomly generated. A structure fingerprinting technique of bond characterization matrix is applied to the generated structures, so that identical structures are strictly forbidden. These procedures significantly enhance the diversity of the structures, which is crucial for structural global search efficiency. Structural searching for each calculation was stopped after generating 1000 ~ 1200 structures (e.g., about 20 ~ 30 generations).

The calculation of elastic constants

The conventional rectangular lattice requires independent elastic constants and strain energy to satisfy the relation: $E_S = \frac{1}{2}C_{11}\varepsilon_{aa}^2 + \frac{1}{2}C_{22}\varepsilon_{bb}^2 + C_{12}\varepsilon_{aa}\varepsilon_{bb} + 2C_{44}\varepsilon_{ab}^2$, where Es is the strain energy (the total energy of the strained state minus that of the equilibrium state) per unit area, $\varepsilon_{aa,}$ and ε_{bb} are the small strains along the **a** and **b** directions in the harmonic regime, and ε_{ab} is the shear strain. C_{11}, C_{22}, C_{12}, and C_{44} are the independent elastic constants, corresponding to the second partial derivative of strain energy with respect to the applied strain. the strain ε parallel to θ (θ is the angle with respect to **a** direction) direction ε and the strain ε perpendicular to the θ direction $\varepsilon_{\perp}$ induced by the unit stress

σ (θ) can be expressed as

$$\varepsilon_{\parallel} = \frac{C_{11}sin^4\theta + C_{22}cos^4\theta - 2C_{12}sin^2\theta cos^2\theta}{C_{11}C_{22} - C_{12}^2} + \frac{sin^2\theta cos^2\theta}{C_{66}}$$

$$\varepsilon_{\perp} = \frac{(C_{11} + C_{22})sin^2\theta cos^2\theta - C_{12}(sin^4\theta + cos^4\theta)}{C_{11}C_{22} - C_{12}^2} - \frac{sin^2\theta cos^2\theta}{C_{66}}$$

, respectively. Thus, the orientation-dependent Young's modulus (Y(θ)) and Poisson's ratio (ν(θ)) can

be obtained via the following equations:

$$Y(\theta) = \frac{\sigma}{\varepsilon_{\parallel}} = \frac{C_{11}C_{22} - C_{12}^2}{C_{11}sin^4\theta + C_{22}cos^4\theta + \left(\frac{C_{11}C_{22} - C_{12}^2}{C_{66}} - 2C_{12}\right)sin^2\theta cos^2\theta} \quad (S1)$$

$$\nu(\theta) = -\frac{\varepsilon_{\perp}}{\varepsilon_{\parallel}} = \frac{C_{12}(sin^4\theta + cos^4\theta) - \left(C_{11} + C_{22} - \frac{C_{11}C_{22} - C_{12}^2}{C_{66}}\right)sin^2\theta cos^2\theta}{C_{11}sin^4\theta + C_{22}cos^4\theta + \left(\frac{C_{11}C_{22} - C_{12}^2}{C_{66}} - 2C_{12}\right)sin^2\theta cos^2\theta} \quad (S2)$$

, respectively.

● Atomic configurations for C_3N, C_2N, and T-C_3N_2.

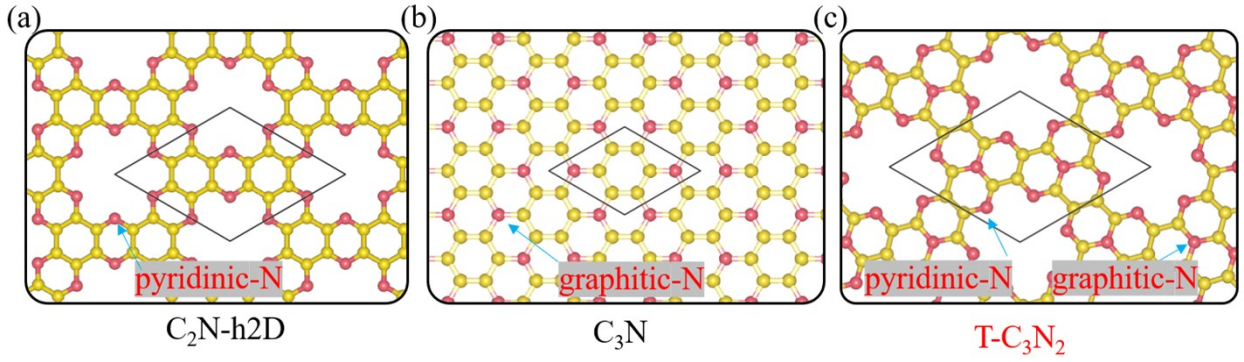

Fig. S5 Atomic configurations for (a) C_3N, (b) C_2N-h2D, and (c) T-C_3N_2. The blue and black balls indicate nitrogen and carbon atoms, respectively. The unit cell is shown by black solid lines.

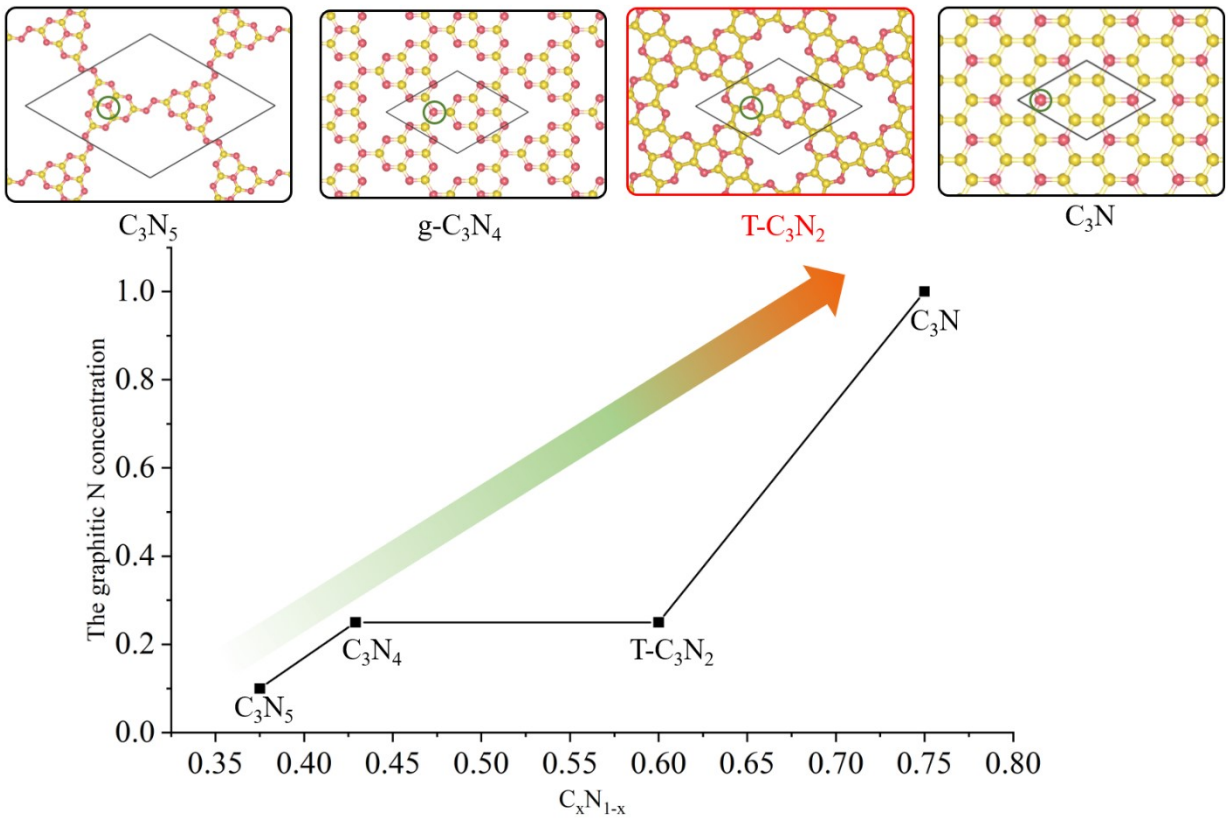

Figure S6. The graphitic N concentration of C_3N_5, g-C_3N_4, T-C_3N_2, and C_3N.

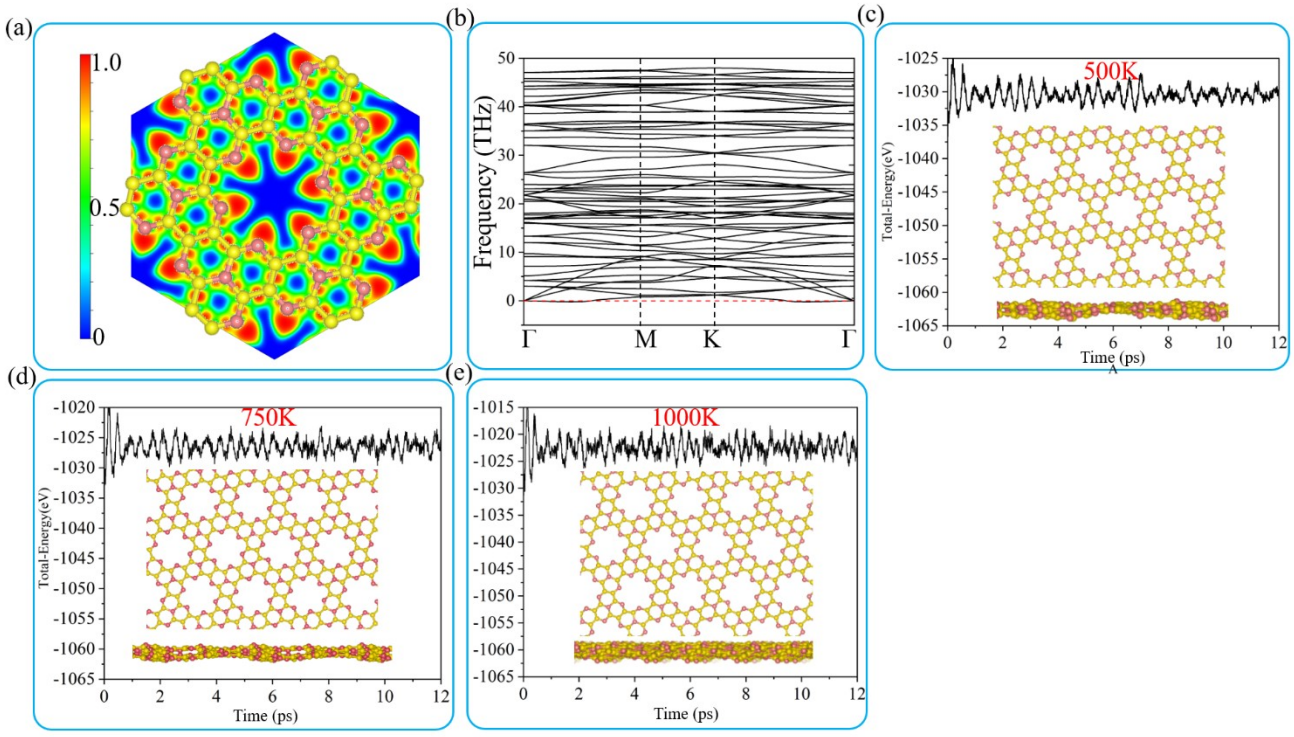

Figure S7. (a) a slice (crossing the monatomic thick structure) of the electron localization function (ELF) of the T-C_3N_2 monolayer. (b) Phonon spectra of the T-C_3N_2 monolayer. (c-e) The final snapshot frame of the T-C_3N_2 monolayer during the AIMD simulation at 500K, 750K, and 1000 K.

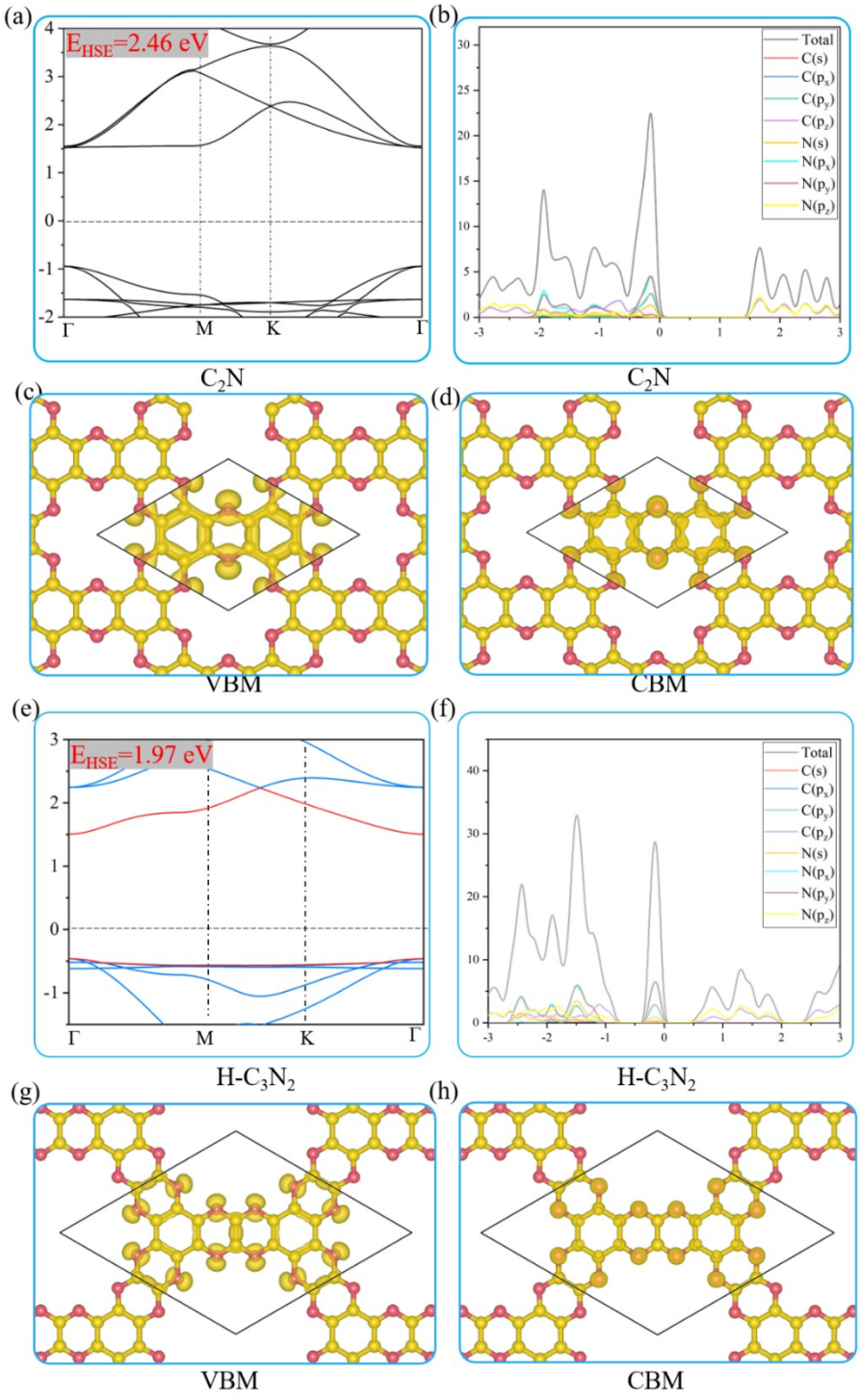

Figure S8. Electronic structures under HSE06 method and the DOS under PBE method of (a-b) C_2N-

h2D monolayer and (e-f) H-C_3N_2. The transverse dotted line is the Fermi energy. Partial charge densities (top view) of the CBM and VBM of (c-d) C_2N-h2D monolayer and (g-h) H-C_3N_2 (isovalue 0.004 e bohr^{-3}).

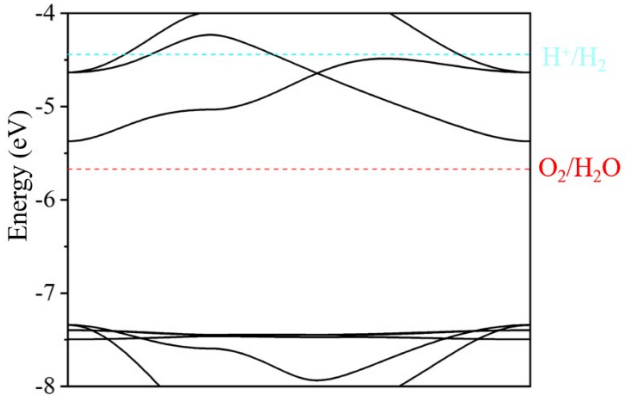

Figure S9. The band structure of H-C_3N_2 relative to the vacuum level. The cyan and red dotted lines indicate the reduction force of hydrogen and the oxidation force of oxygen, respectively.

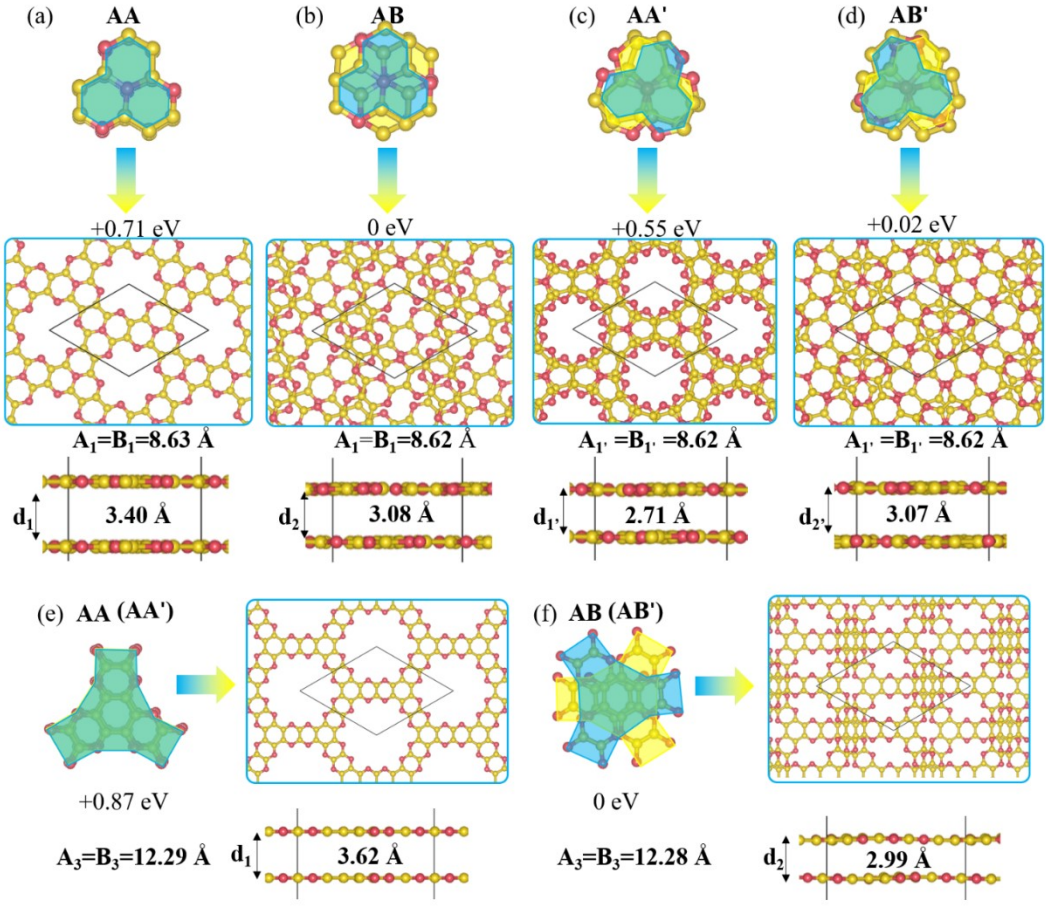

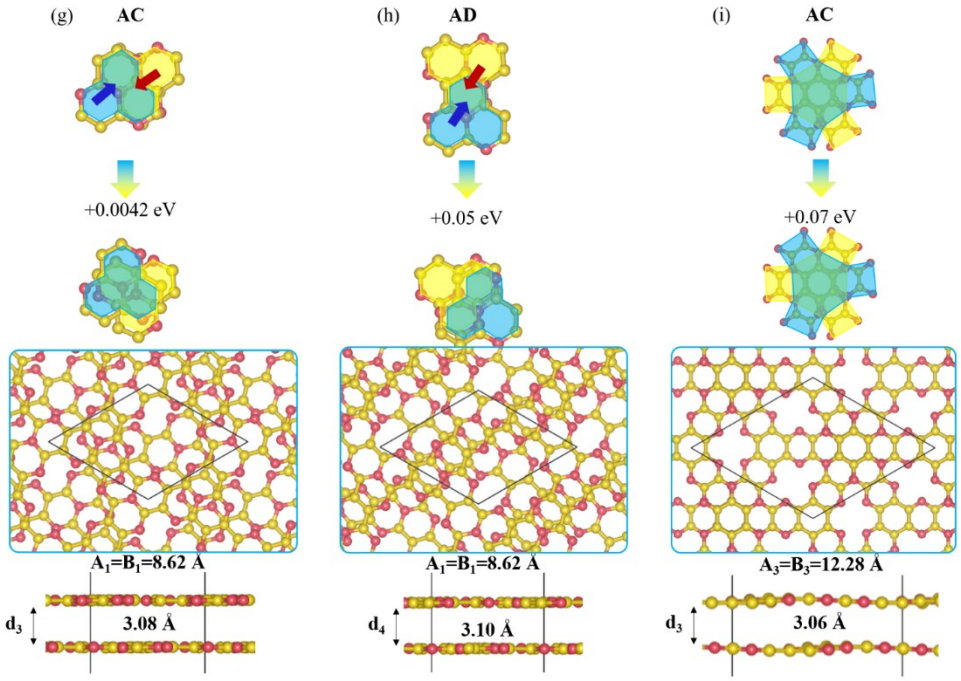

Figure S10. The different stacking bilayers of H-C_3N_2 and T-C_3N_2. (a-d) Configurations of AA, AB, AA', and AB' T-C_3N_2 on top views (upper panel) and side views (lower panel) (e-f) Configurations of AA (AA') and AB (AB') H-C_3N_2 on top views (upper panel) and side views (lower panel). The energy is the energy difference between the most favorable bilayer H-C_3N_2 (T-C_3N_2) and the others. (g-h) Configurations of AC and AD bilayers of T-C_3N_2 on top views (upper panel) and side views (lower panel). (i) Configurations of AC bilayer of H-C_3N_2 on top views (upper panel) and side views (lower panel). A_1, B_1, $A_{1'}$, $B_{1'}$, A_3, and $B_{3'}$ are the corresponding lattice parameters. d_1, d_2, $d_{1'}$, $d_{2'}$, d_3 and d_4 are the interlayer spacing.

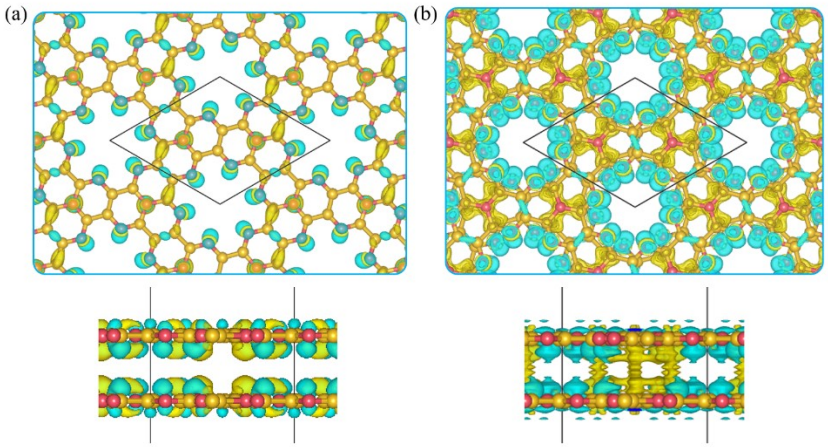

Figure S11. Top and side views of the differential charge density of (a) AA and (b) AA' stacking bilayers T-C_3N_2 with an isosurface value of 0.0004 e Bohr^{-3}.

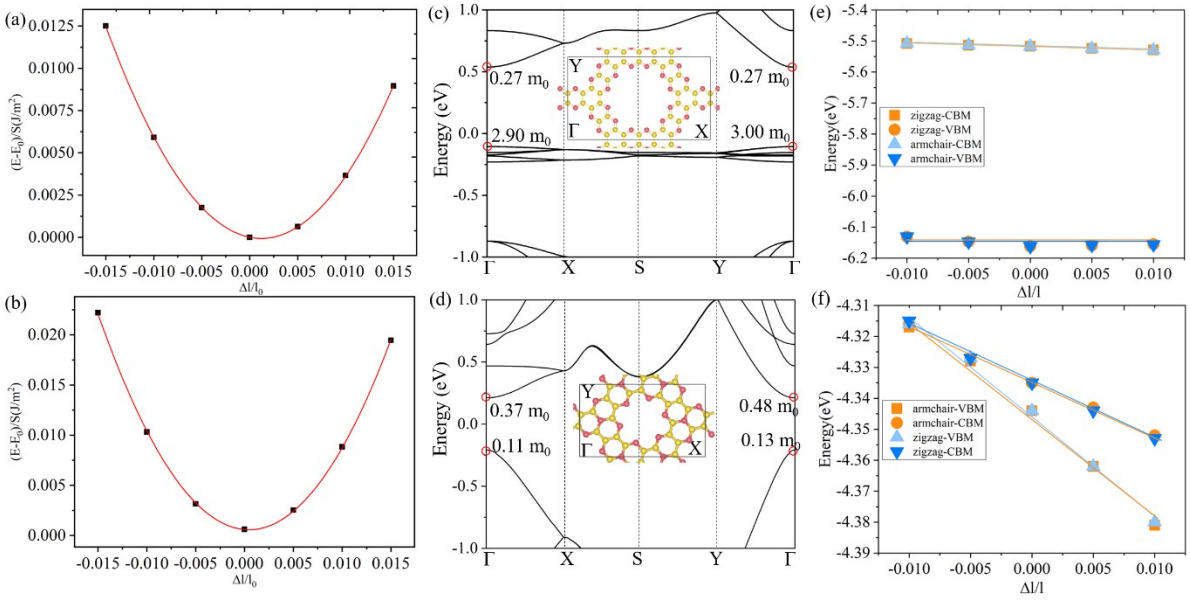

Figure S12. (a-b) Total energy shift E-E_0 on the per surface as a function of lattice deformation Δl/l along **a** and **b** directions in T-C_3N_2 and H-C_3N_2. (c-d) The effective mass of T-C_3N_2 and H-C_3N_2 in **a**(**b**) direction in CBM and VBM. (e-f) Relationship between energy shift of the band edge position and the dilation Δl/l.

References

1. K. Maeda, X. Wang, Y. Nishihara, D. Lu, M. Antonietti and K. Domen, *J. Phys. Chem. C*, 2009, **113**, 4940-4947.
2. S. C. Yan, Z. S. Li and Z. G. Zou, *Langmuir*, 2009, **25**, 10397-10401.
3. H. Ji, F. Chang, X. Hu, W. Qin and J. Shen, *Chem. Eng. J.*, 2013, **218**, 183-190.
4. G. Zhang, J. Zhang, M. Zhang and X. Wang, *J. Mater. Chem.*, 2012, **22**, 8083.
5. F. Dong, Z. Wang, Y. Sun, W.-K. Ho and H. Zhang, *J. Colloid Interface Sci.*, 2013, **401**, 70-79.
6. A. B. Jorge, D. J. Martin, M. T. S. Dhanoa, A. S. Rahman, N. Makwana, J. Tang, A. Sella, F. Cora, S. Firth, J. A. Darr and P. F. McMillan, *J. Phys. Chem. C*, 2013, **117**, 7178-7185.
7. R. Walczak, B. Kurpil, A. Savateev, T. Heil, J. Schmidt, Q. Qin, M. Antonietti and M. Oschatz, *Angew. Chem. Int. Ed. Engl.*, 2018, **57**, 10765-10770.
8. A. Riano, K. Strutynski, M. Liu, C. T. Stoppiello, B. Lerma-Berlanga, A. Saeki, C. Marti-Gastaldo, A. N. Khlobystov, G. Valenti, F. Paolucci, M. Melle-Franco and A. Mateo-Alonso, *Angew. Chem. Int. Ed. Engl.*, 2021, **60**, 2-9.
9. X. Hu, L. Zhong, C. Shu, Z. Fang, M. Yang, J. Li and D. Yu, *J. Am. Chem. Soc.*, 2020, **142**, 4621-4630.
10. J. Xu, J. Mahmood, Y. Dou, S. Dou, F. Li, L. Dai and J. B. Baek, *Adv. Mater.*, 2017, **29**, 1702007-1702014.
11. J. Mahmood, F. Li, S. M. Jung, M. S. Okyay, I. Ahmad, S. J. Kim, N. Park, H. Y. Jeong and J. B. Baek, *Nat. Nanotechnol.*, 2017, **12**, 441-446.
12. Q. M. Bing, W. Liu, W. C. Yi and J. Y. Liu, *J. Power Sources*, 2019, **413**, 399-407.
13. Z. Meng, A. Aykanat and K. A. Mirica, *Chem. Mater.*, 2018, **31**, 819-825.
14. Z.-Q. Lin, J. Xie, B.-W. Zhang, J.-W. Li, J. Weng, R.-B. Song, X. Huang, H. Zhang, H. Li, Y. Liu, Z. J. Xu, W. Huang and Q. Zhang, *Nano Energy*, 2017, **41**, 117-127.
15. C. Ma, X. Li, J. Zhang, Y. Liu and J. J. Urban, *ACS Appl. Mater. Inter.*, 2020, **12**, 16922-16929.
16. X. Li, H. Wang, H. Chen, Q. Zheng, Q. Zhang, H. Mao, Y. Liu, S. Cai, B. Sun, C. Dun, M. P. Gordon, H. Zheng, J. A. Reimer, J. J. Urban, J. Ciston, T. Tan, E. M. Chan, J. Zhang and Y. Liu, *Chem*, 2020, **6**, 933-944.
17. I. Ahmad, F. Li, C. Kim, J.-M. Seo, G. Kim, J. Mahmood, H. Y. Jeong and J.-B. Baek, *Nano Energy*, 2019, **56**, 581-587.
18. L. Meng, S. Ren, C. Ma, Y. Yu, Y. Lou, D. Zhang and Z. Shi, *Chem. Commun.*, 2019, **55**, 9491-9494.
19. R. Shi, L. Liu, Y. Lu, C. Wang, Y. Li, L. Li, Z. Yan and J. Chen, *Nat. Commun.*, 2020, **11**, 178.
20. J. Mahmood, I. Ahmad, M. Jung, J.-M. Seo, S.-Y. Yu, H.-J. Noh, Y. H. Kim, H.-J. Shin and J.-B. Baek, *Commun. Chem.*, 2020, **3**, 31.
21. J. Park, M. Lee, D. Feng, Z. Huang, A. C. Hinckley, A. Yakovenko, X. Zou, Y. Cui and Z. Bao, *J. Am. Chem. Soc.*, 2018, **140**, 10315-10323.
22. C. Li, L. Shi, L. Zhang, P. Chen, J. Zhu, X. Wang and Y. Fu, *J. Mater. Chem. A*, 2020, **8**, 369-379.
23. A. C. Hinckley, J. Park, J. Gomes, E. Carlson and Z. Bao, *J. Am. Chem. Soc.*, 2020, **142**, 11123-11130.

24. D. Xing, Y. Wang, P. Zhou, Y. Liu, Z. Wang, P. Wang, Z. Zheng, H. Cheng, Y. Dai and B. Huang, *Appl. Catal., B*, 2020, **278**.
25. T. Chen, J.-H. Dou, L. Yang, C. Sun, N. J. Libretto, G. Skorupskii, J. T. Miller and M. Dinca, *J. Am. Chem. Soc.*, 2020, **142**, 12367-12373.
26. R. Iqbal, S. Ali, G. Yasin, S. Ibraheem, M. Tabish, M. Hamza, H. Chen, H. Xu, J. Zeng and W. Zhao, *Chem. Eng. J.*, 2022, **430**, 132642.
27. X. Cai, W. Yi, J. Chen, L. Lu, B. Sun, Y. Ni, S. A. T. Redfern, H. Wang, Z. Chen and Y. Chen, *J. Mater. Chem. A*, 2022, **10**, 6551–6559.
28. J. Mahmood, E. K. Lee, M. Jung, D. Shin, I. Y. Jeon, S. M. Jung, H. J. Choi, J. M. Seo, S. Y. Bae, S. D. Sohn, N. Park, J. H. Oh, H. J. Shin and J. B. Baek, *Nat. Commun.*, 2015, **6**, 6486-6492.
29. C. Shu, L. Fang, M. Yang, L. Zhong, X. Chen and D. Yu, *Angew. Chem. Int. Ed. Engl.*, 2021, **134**.
30. O. Buyukcakir, R. Yuksel, Y. Jiang, S. H. Lee, W. K. Seong, X. Chen and R. S. Ruoff, *Angew. Chem. Int. Ed.*, 2019, **58**, 872-876.
31. Y. Wang, J. Lv, L. Zhu and Y. Ma, *Comput. Phys. Commun.*, 2012, **183**, 2063-2070.
32. Y. C. Wang, J. A. Lv, L. Zhu and Y. M. Ma, *Phys. Rev. B*, 2010, **82**, 094116-094123.
33. G. Kresse and J. Furthmüller, *Phys. Rev. B*, 1996, **54**, 11169-11186.